Fatigue Crack Initiation in the Iron-Based Shape Memory Alloy FeMnAlNiTi

R. Sidharth[1] · W. Abuzaid[2] · M. Vollmer[3] · T. Niendorf[3] · H. Sehitoglu[1]

Abstract The newly developed FeMnAlNiTi shape memory alloy (SMA) holds significant promise due to its desirable properties including ease of processing, room temperature superelasticity, a wide superelastic window of operation, and high transformation stress levels. In this study, we report single crystals with tensile axis near $\langle 123 \rangle$ exhibiting transformation strains of 9% with a high transformation stress of 700 MPa. The functional performance revealed excellent recovery of 98% of the applied strain in an incremental strain test for each of the 40 applied cycles. Concomitantly, the total residual strain increased after each cycle. Accumulation of residual martensite is observed possibly due to pinning of austenite/martensite (A/M) interface. Subsequently, under structural fatigue loading with a constant strain amplitude of 1%, the recoverable strains saturate around 1.15% in local residual martensite domains. Intermittent enhancement of recoverable strains is observed due to transformation triggered in previously untransformed domains. Eventually, fatigue failure occurred after 2046 cycles and the dominant mechanism for failure was microcrack initiation and coalescence along the A/M interface. Thus, it is concluded that interfacial dislocations, which play a crucial role in the superelastic (SE) functionality, invariably affect the structural fatigue performance by acting as the weakest link in the microstructure.

✉ R. Sidharth
ravi8@illinois.edu

H. Sehitoglu
huseyin@illinois.edu

[1] Department of Mechanical Science and Engineering, University of Illinois At Urbana-Champaign, 1206 W. Green St., Urbana, IL 61801, USA

[2] Department of Mechanical Engineering, American University of Sharjah, PO Box 26666, Sharjah, United Arab Emirates

[3] Institute of Materials Engineering, University of Kassel, Mönchebergstraße 3, 34125 Kassel, Germany

Introduction

NiTi-based shape memory alloys (SMAs) are the most widely used SMAs to date due to their large transformation strains and good functional stability when subjected to cycling loading [1–3]. However, extended commercial usage of NiTi is still hindered by the relatively low transformation stress levels and high cost of production. Thus, various Iron-based SMAs have gained a lot of attention owing to better workability and lower processing costs. Fe-based SMAs are particularly attractive for load bearing applications, such as prestressing tendons and seismic damping of earthquake resistant structures, which require high tensile strength [4–6]. Up to now, research has been focused on Fe-SMAs like FeNiCoTi [7–9], FePd [10], FeMnSi [11, 12], FeNiCoAlX (X = Ti, Ta, or Nb) [13–15] and FeMnAlNi [16–20]. Especially, the recently developed FeMnAlNi alloy system is of immense interest due to its superior superelastic (SE) properties at room temperature [19], i.e., transformation strains up to 12% [21–23] and

transformation stresses reaching up to 600 MPa [21, 23]. Additionally, a weak temperature dependence of transformation stress over a large temperature window (> 400 °C) is characteristic for the alloy [21]. However, the functionality of this alloy system is extremely sensitive to grain size, grain orientation, aging, and the resulting precipitate size [18, 24, 25]. In general, achieving SE in FeMnAlNi requires a coarse oligocrystalline microstructure due to its susceptibility for grain boundary cracking. The aforementioned microstructure is achieved via a cycle heat treatment (CHT) procedure which induces abnormal grain growth (AGG) [26]. Additionally, a final water quench from the α single phase region is needed to retain the austenite at RT for superelastic applications [27]. However, studies show that FeMnAlNi is highly sensitive to the quenching rate, which can lead to crack formation along the grain boundaries if cooling is too fast and to the formation of undesirable gamma phase if cooling is too slow [28]. The near perfect quenching conditions, which needs to be warranted, constrain the sample dimensions where SE can be realized and therefore limits the practical applicability of this attractive SMA.

To circumvent this issue, Vollmer et al. alloyed FeMnAlNi with 1.5 at.% Ti and produced an alloy with the nominal composition of $Fe_{42}Mn_{34}Al_{15}$ $Ni_{7.5}Ti_{1.5}$ (at.%) [29]. They were able to affect the precipitation in such a way that air cooling was sufficient to generate a thin film of gamma phase at the grain boundaries. Furthermore, as reported in a second study [30], Ti changes the morphology of the γ phase and thereby accelerates AGG. By employing CHT, a large 220 mm long and 6.3 mm diameter single crystal was grown. Transformation strains as high as 8% were observed and the transformation stress exceeded 800 MPa. Compression strength, on the other hand, exceeded 1.6 GPa and the corresponding fracture strain exceeded 10% [29]. Moreover, Vollmer et al. [30] were able to achieve superelasticity in large 100 mm long and 6 mm diameter rods owing to the enhanced AGG and low quenching sensitivity of this alloy system. In light of the high work output due to large transformation strains and stresses combined with the ease of processing large samples which exhibit room temperature SE, FeMnAlNiTi shows considerable promise for a wide range of engineering applications.

Notwithstanding all the favorable properties of Fe-based SMAs, they suffer from poor functional performance under fatigue loading. The irreversibility of the transformation has been attributed to extensive plastic deformation at the austenite martensite interface [31, 32]. The reverse motion of the A/M interface is facilitated by shrinkage of the internal twins via the migration of twinning partials which inevitably leave behind residual dislocations in the austenite matrix [33]. These dislocations pin the A/M interface and lead to strain accumulation in the form of residual martensite. Experimental observations by Kajiwara focusing on diverse SMAs [31, 33, 34] show that the interfacial dislocations are aligned with the twinning shear direction of the internally twinned martensite. Together with Kajiwara's TEM observations and the topological model of twin boundary migration [35], the interfacial dislocations have been proposed to arise from a dislocation reaction occurring at the A/M interface and the twinning partial during reverse motion of the interface [36]. Despite of the different transformation path in FeMnAlNi, similar dislocations were observed in FeMnAlNi single crystals in incremental strain tests [23] as well as in functional fatigue tests [37]. Given that the interfacial dislocations play a crucial role in the functional degradation of Fe-based SMAs over cycling loading, it is expected to also impact structural fatigue performance. For load bearing applications, the structural fatigue performance is crucial. Recent study [38] on the fatigue crack growth in superelastic FeMnAlNi has shown that the crack growth response is highly influenced by the activated martensite variants at the crack tip. However, the functional fatigue and crack initiation processes are still unclear. Similar to dislocation pile-ups at grain boundaries in polycrystalline metals, the dislocation rich A/M interface in Fe-based SMAs could act as fatigue crack initiation sites. Unambiguous experimental confirmation of such a mechanism for fatigue crack initiation in SMAs is missing till date. On the other hand there has been concerted efforts on fatigue crack growth driving forces [1, 39–42].

In the current study, the room temperature stress–strain response of superelastic FeMnAlNiTi single crystal was characterized in uniaxial tension. The loading direction of the single crystals was obtained by Electron Backscatter Diffraction (EBSD) technique. Dislocation-induced lattice reorientation was evidenced by carrying out EBSD after the tension test. Functional performance of the alloy was studied in an incremental strain test under an applied strain increment of 1% for 40 cycles. The degradation of the superelastic strains was characterized using in situ digital image correlation (DIC). Afterwards, the structural fatigue performance of the same sample that underwent functional fatigue was studied under an applied total strain range of 1%. Intermittent enhancement of superelasticity, in the form of a sharp increase in the magnitude of SE strains, was observed during cycling loading. After fatigue fracture, the samples were characterized using scanning electron microscopy (SEM). Residual martensite was found, and interfacial cracking was observed as a mechanism for fatigue crack initiation in this Fe-SMA.

Experimental methodology

Dogbone-shaped samples having a 2 mm wide and 1.2 mm thick cross section were electro-discharge machined out of a single crystalline $Fe_{42}Mn_{34}Al_{15}Ni_{7.5}Ti_{1.5}$ (at%) ingot. The ingot was prepared via induction melting and grown into a single crystal by inducing AGG via CHT [30]. The dogbone samples were encapsulated in quartz tubes with a residual argon pressure < 50 mTorr. Afterwards, samples were solutionized at 1225 °C for 30 min and quenched in air by breaking the tube. The samples were polished down to 4000P SiC abrasive papers, followed by wet polishing in 1 μm suspended alumina and then finally vibro-polished in 0.02 μm suspended silica to obtain satisfactory surface quality for EBSD. Subsequently, the loading direction of the sample was determined to be close to ⟨123⟩. Full-field strain measurements were conducted using DIC following standard sample preparation procedures as detailed in [43].

An Instron servo-hydraulic load frame was used to conduct mechanical tests by loading under strain control with an average strain rate of 10^{-3} s^{-1} using an extensometer (5 mm gauge length) and unloading in load control with a rate of 25 N s^{-1}. The uniaxial tension test was performed up to 8% applied strain. To evaluate the functional fatigue performance of the considered Fe-based SMA, a specimen was subjected to cyclic loading, with 1% applied strain per cycle, i.e., the total applied strain was increased each cycle incrementally. A total of 40 cycles were applied with focus on functional properties. The superelastic response was evaluated using in situ DIC with focus on both the global (i.e., average response from entire gauge section) and the local levels (i.e., local region within the sample). Throughout the experiment, a 7 × 2 mm^2 area of interest was monitored with deformation images captured every 2 s. Following the initial functional cycling, the loading rate (strain control) was increased to 0.75 Hz which was sustained to sample failure. The loading rate was increased to allow for a significantly larger number of cycles which would induce the initiation of fatigue cracks and structural failure. During this phase of the experiment, a constant strain range of 1% was maintained, i.e., the total strain was kept constant for every cycle, and optical images were captured at 15 frames s^{-1} to characterize the local strain response under fatigue loading. After fatigue fracture, the samples were again polished for microstructural characterization using SEM.

Results and discussion

Uniaxial response

During a quasi-static tensile test, under strain control, a macroscopic recoverable strain of 8% was observed on the global scale in an FeMnAlNiTi single crystal in the current study (Fig. 1). The loading orientation was close to ⟨123⟩ and according to lattice deformation theory, the theoretical transformation strain in tension can be as high as 12% for this orientation [20]. However, the local recoverable strain in the sample reaches only around 9% and, thus, is slightly below the theoretical transformation strain mentioned above, however, in good agreement with theoretical values calculated by the phenomenological theories for FeMnAlNi [18], which takes the formation of twins into account. As previously shown [30], FeMnNiAlTi exhibits higher transformation stress (800 MPa) as compared to FeMnAlNi which could be due to the energy landscape of the transformation pathway exhibiting a higher energy barrier compared to that of FeMnNiAl [20]. Upon unloading, a nearly perfect reversibility was observed on the global scale, whereas a local residual strain of about 0.35% was recorded by DIC. Residual strain is most likely due to the formation of dislocations and the accumulation of residual martensite pinned by interfacial dislocations. The presence of dislocations in the austenite matrix can be inferred from the spread in the IPF map obtained from EBSD post-uniaxial tension test (Fig. 1 inset) and has been already directly revealed for the FeMnAlNi system by in-depth analysis using transmission electron microscopy [23, 37]. Such analysis, however, is beyond the scope of present work and, thus, will be the subject of follow-up studies.

Functional fatigue

After testing the room temperature uniaxial response, the functional performance of the sample was evaluated by loading under strain control up to a maximum strain of 1% and unloading using load control. Each subsequent cycle was subjected to an applied strain of 1%. Eventually, this leads to an incrementally increasing total maximum strain due to the accumulation of residual strains (i.e., the strain range is not constant). This procedure was repeated for 40

Fig. 1 Uniaxial stress strain response of FeMnNiAlTi at RT. The local recoverable strain is around 9% and the residual strain is around 0.35% (see DIC maps at the bottom). The inset depicts the IPF map of the loading direction obtained from EBSD before and after loading
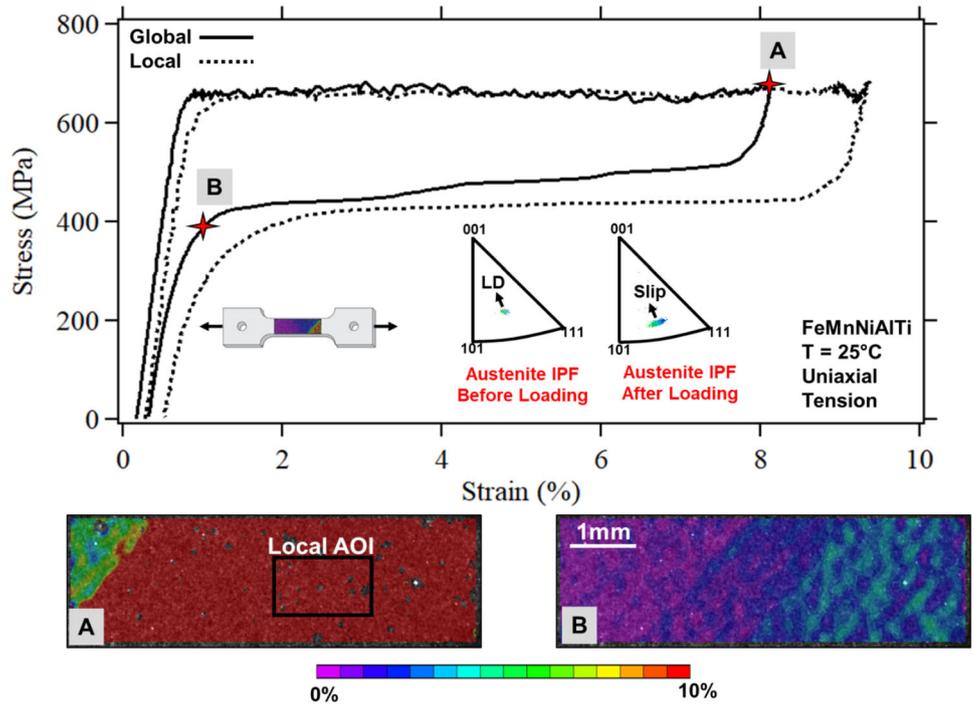

Fig. 2 Functional fatigue of FeMnNiAlTi for 40 cycles under an applied total strain of 1% in an incremental strain test. The inset on the top right displays the schematic of the applied loading. The inset at the bottom right shows recovery in % and macroscopic (global) residual strain accumulation over continued cycling. See text for details
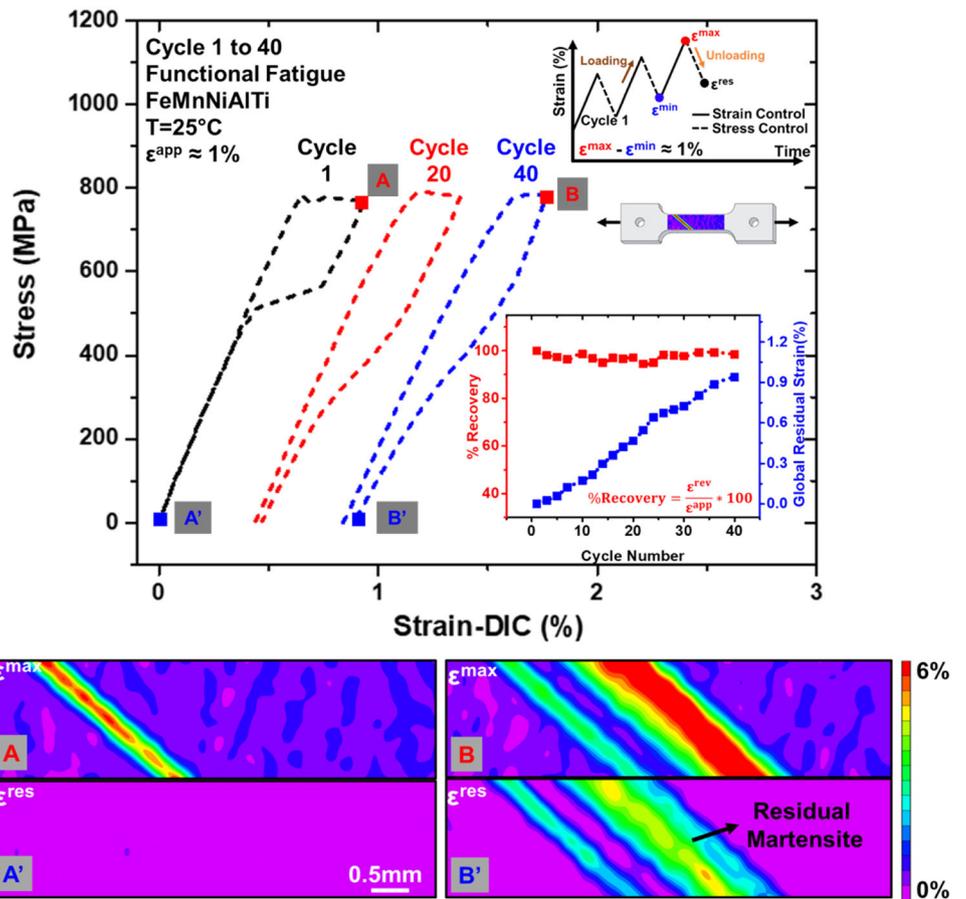
cycles. The results for selected cycles are presented in Fig. 2 (cycles 1, 20, and 40). The hysteresis loops shown in Fig. 2 point to increased hysteresis upon continued cycling indicating defect formation such as dislocations. The macroscopic residual strain is virtually zero in the first cycle due to complete recovery of martensite upon unloading. However, the macroscopic residual strain reaches 0.93% by cycle 40. Even though the residual strains increase at the rate of 0.023% per cycle, the macroscopic recoverability of the material is stable with 98% recovery for the 40 cycles considered in the incremental strain test. Even with the accumulation of residual strains, there is no considerable change in the transformation stress over the 40 applied cycles. Based on previous studies on NiTi systems [1, 44, 45], the transformation stress decreases with cycling. However, and unlike NiTi, the transformation stress is constant in FeMnNiAlTi possibly due to the activation of previously untransformed austenite domains upon cycling. The impact this has on the fatigue response requires further study. The SE functionality is expected to degrade upon continued functional fatigue due to the steady accumulation of residual martensite eventually reducing the volume fraction of functional austenite domains that exhibit higher recoverable strains. The stability of martensite upon unloading is closely linked to the formation of defects at the A/M interface finally affecting its mobility by pinning the interface [23, 33, 34, 37, 46, 47]. This will inevitably

Fig. 3 Structural fatigue of FeMnNiAlTi from cycle 41 to 2046 (failure). **a** Stress–strain curves plotted using the extensometer strain indicating no ratcheting (only plotted for cycles 50 to 2046 for clarity). The inset shows the schematic highlighting the applied loading. **b** Stress–strain curve plotted using DIC strains indicating that the sample ratchets. **c** The hysteresis loops separated for clarity. The inset depicts the comparison of DIC vs Extensometer stress–strain curves at cycle 500. Note that DIC captures the hysteresis precisely
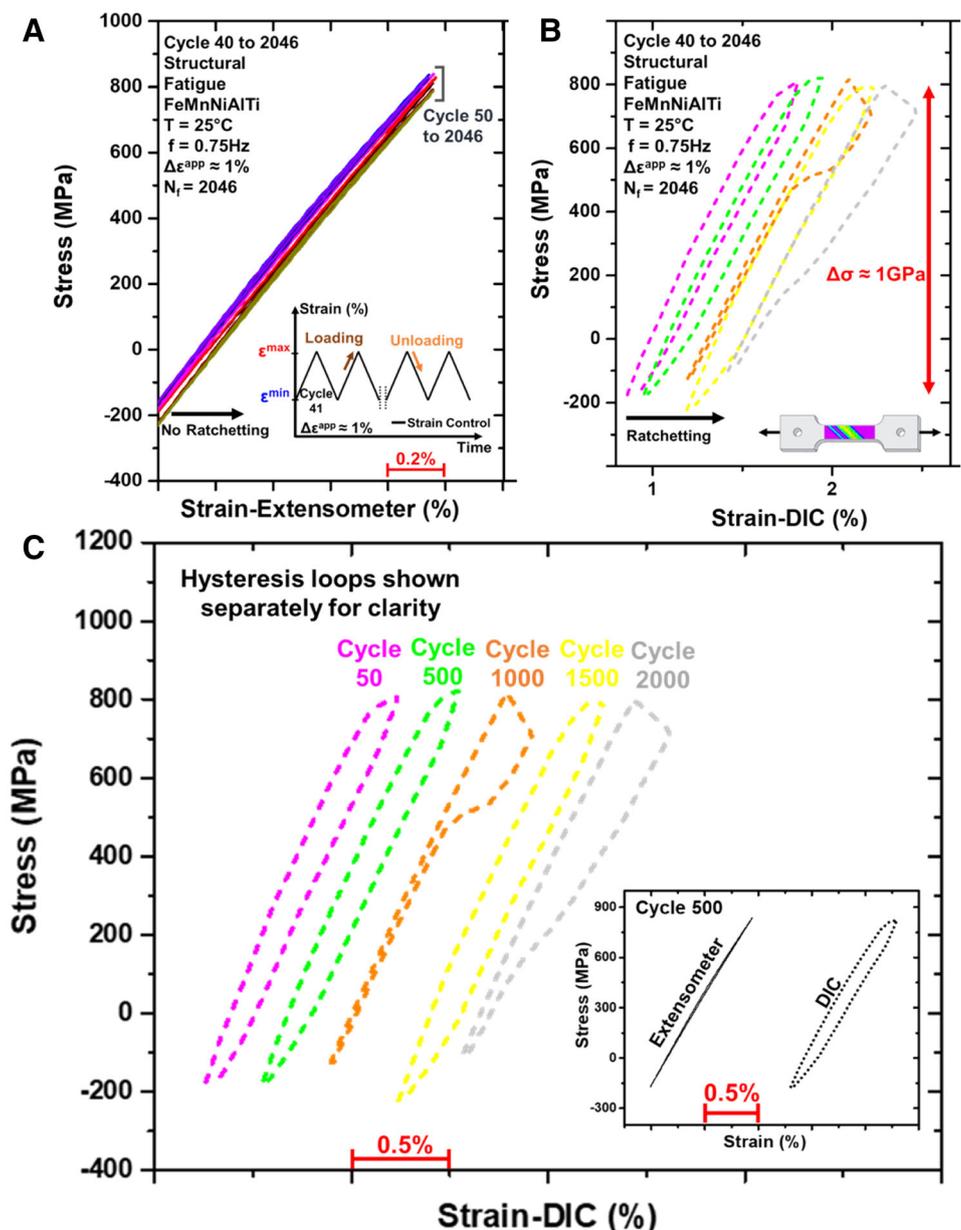
influence the structural fatigue performance of the alloy as discussed below.

Structural fatigue

The structural fatigue response of the material under a total applied strain range of 1% is shown in Fig. 3. As cycling was done only in strain control here, already within the first few cycles, compressive stresses are seen upon unloading (as will be discussed further below). From cycle 40 to cycle 50, the superelastic response diminishes and the global response of the entire sample seems completely elastic, without any ratcheting (Fig. 3a, cycles 40 to 50 are omitted for clarity). However, ratcheting was observed when using the strain obtained from global DIC measurements (global

AOI is the entire DIC window shown in Fig. 4). At this point, it should be noted that the gage length of the DIC AOI is > 6 mm and that of extensometer is ≈ 5 mm. One potential factor of the observed ratcheting could be the strain contribution from sample areas outside the gage length of the extensometer. Nevertheless, the residual martensite domain (local AOI of approximately 0.2×0.2 mm^2 in Fig. 4) exhibits recoverable strains of around 1.15%. Thus, each fatigue cycle involves growth and shrinkage of the thin martensite plates which are present in the residual martensite domains (cf. Fig. 5). This eventually leads to the accumulation of interfacial defects that act to pin the A/M interface and contribute to the hysteresis captured by the stress–strain loops plotted from DIC (Fig. 3b). In consequence, the microstructure

Fig. 4 The local recoverable strains and the macroscopic (global) residual strains plotted versus the cycle number for structural fatigue. Note that the local recoverable strains saturated at 1.15%, however, intermittent spikes in recoverable strains are observed due to activation of new volumes of material. Subsequently, the global residual strains increase due to the accumulation of residual martensite in the newly activated region. Note that the global AOI is the entire DIC window
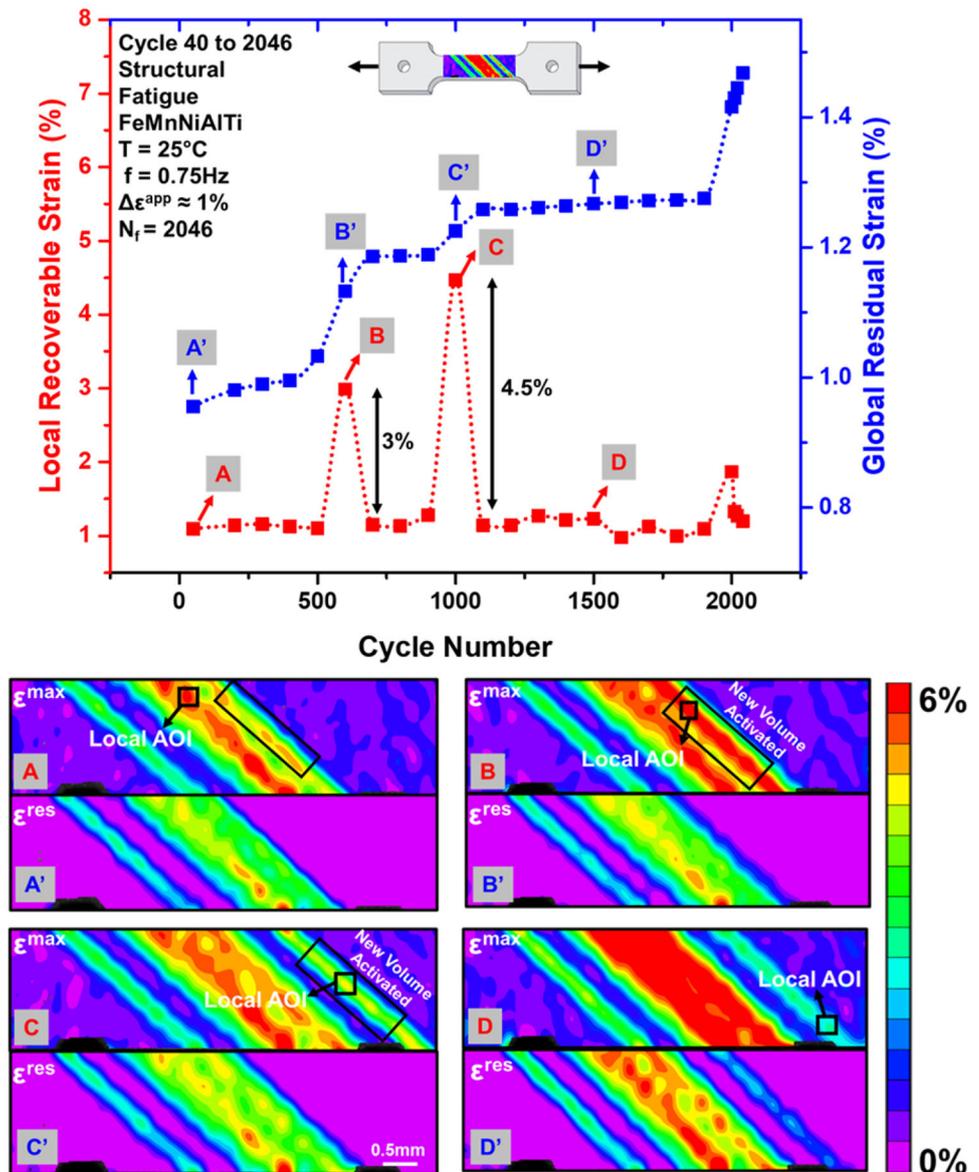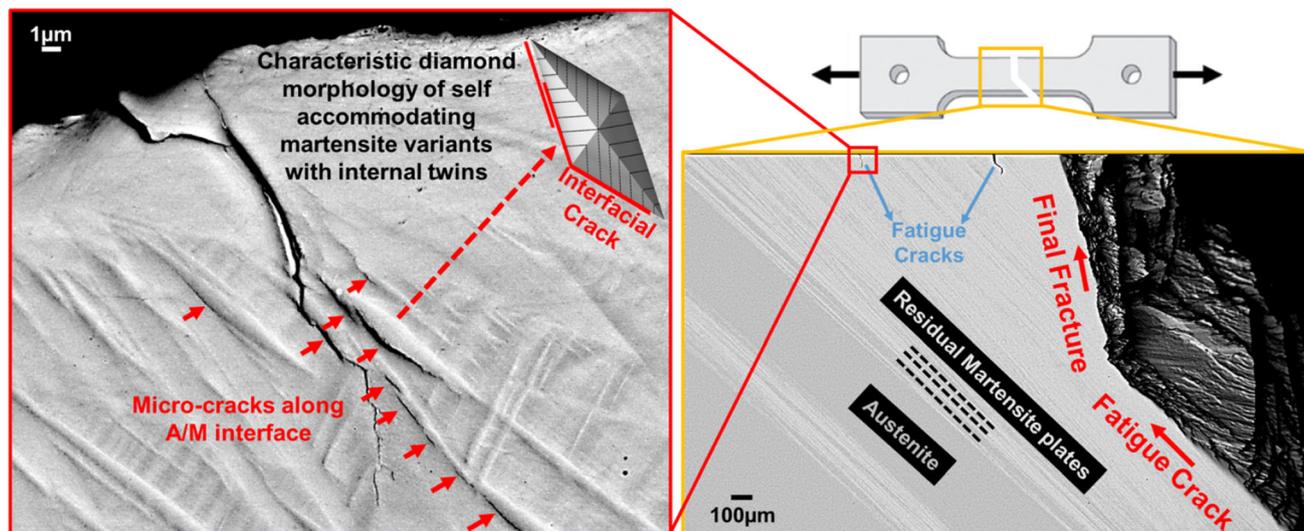
Fig. 5 SEM-BSE image of the sample surface post-fatigue fracture. The low-magnification image on the right shows the residual martensite near the fatigue crack. The fatigue crack has propagated parallel to the activated martensite variant. A high-magnification image of the other fatigue cracks near the sample edge taken at × 35,000 is shown on the left. Several microcracks have formed along the A/M interface

evolution forces the sample to go into compression to facilitate strain reversal and maintain the applied strain range. Concomitantly, the stress response of the sample drastically spikes to about 950 MPa in the 50th cycle and gradually increases thereafter to about 1 GPa (Fig. 3b). Around cycle 600, transformation is triggered in the previously untransformed domains of sample (Fig. 4), most possibly due to internal stress build-up induced by the accumulation of interfacial defects. The progressive transformation of previously untransformed areas was also observed in functional fatigue tests in FeMnAlNi [37, 48]. It was found that the interplay of different degradation mechanisms leads to a partially inhibited reactivation of already transformed areas and, thus, to the transformation of previously untransformed areas. This transformation is characterized by a jump in the local recoverable strains in the present study (Fig. 4). The recoverable strains reach as high as 4.5% locally, far above the nominal level of 1.15%, following the activation of new transformation regions. This intermittent enhancement of superelasticity was observed around cycle 600, 1000, and 2000.

The sample eventually suffered fatigue failure after 2046 fatigue cycles. Optically the fatigue crack was observed to initiate and propagate parallel to the accumulated residual martensite variants. Post fatigue failure, SEM-BSE images (Fig. 5) of the sample surface unambiguously reveal that the fatigue crack propagated parallel to the activated martensite variant. The higher magnification SEM-BSE image taken at × 35,000 (Fig. 5) uncovers several microcracks decorated along the A/M interface of the dominant martensite variant (Fig. 4). This suggests that

the fatigue crack initiation occurred at the A/M interface. It should be noted that, in the past, there have been significant efforts on understanding slip localization at the A/M interface [31, 33, 34]. Thus, considering these previous studies, a possible mechanism for fatigue crack initiation is discussed further below.

During fatigue loading, the growth and shrinkage of martensite plates in the local volume of the sample occur via the motion of the A/M interface. The mobility of the A/M interface is facilitated by the movement of the twin boundary (TB) of the internally twinned martensite [35, 36]. Additionally, it has been previously shown that the parallel dislocation loops present at the A/M interface extend along the twinning shear direction of the internal twins [33, 34, 49]. Following such observations, Kajiwara [33, 34] proposed that a dislocation reaction between the twinning partial that resides on the internal TB and the A/M interface is the source of the interfacial dislocations for several SMAs. This mechanism is further enunciated in the model of Sehitoglu-Mohammed [36, 50]. At this point, it has to be noted that all the SMAs studied above are characterized by a different transformation path compared to the FeMnAlNiTi alloy studied here. However, in case of the FeMnAlNiTi sample studied in present work, it is assumed that a similar mechanism prevails. Thus, the continued forward and reverse movement and the associated slip emission at the A/M interface during structural cycling are expected to act as a stress concentrator and lead to microcrack initiation. Ensuing crack growth is proposed to occur via microcrack coalescence along the A/M interface.

Conclusion

This work supports the following conclusions:

1. FeMnAlNiTi is extremely promising among the Fe-based SMAs due to its room temperature SE with transformation stress as high as 800 MPa, 9% recoverable strain, and the ease of processing to produce a microstructure with large grains conducive for functionality.
2. The SE functionality tested under 1% applied strain for 40 cycles in an incremental strain test reveals stable performance with excellent recoverability (98%). However, residual strain accumulation is observed due to the accumulation of residual martensite probably pinned by interfacial dislocations in the austenite matrix.
3. The effect of the initial functional cycling for 40 cycles on the structural fatigue performance was tested under an applied total strain range of 1%. It was observed that the local recoverable strains in the residual martensite domains reached 1.15% for most cycles. However, intermittent enhancement of recoverable strains (as high as 4.5%) was observed due to the activation of previously untransformed austenite domains of the sample. Subsequently, the sample ratchets due to the accumulation of residual martensite in those domains.
4. Fatigue failure occurred after 2046 cycles. The dominant failure mechanism was identified as microcrack initiation and coalescence along the A/M interface. It is proposed that the interfacial dislocations, which play a crucial role in the SE functionality of Fe-SMAs, invariably affects the structural fatigue performance by acting as the weakest link in the microstructure.

References

1. Eggeler G, Hornbogen E, Yawny A, Heckmann A, Wagner M (2004) Structural and functional fatigue of NiTi shape memory alloys. Mater Sci Eng A 378(1–2):24–33
2. Lagoudas DC (2008) Shape memory alloys: modeling and engineering applications. Springer, New York
3. Sehitoglu H, Patriarca L, Wu Y (2017) Shape memory strains and temperatures in the extreme. Curr Opin Solid State Mater Sci 21(2):113–120
4. Cladera A, Weber B, Leinenbach C, Czaderski C, Shahverdi M, Motavalli M (2014) Iron-based shape memory alloys for civil engineering structures: an overview. Constr Build Mater 63:281–293
5. Janke L, Czaderski C, Motavalli M, Ruth J (2005) Applications of shape memory alloys in civil engineering structures—overview, limits and new ideas. Mater Struct 38(5):578–592
6. Izadi M, Motavalli M, Ghafoori E (2019) Iron-based shape memory alloy (Fe-SMA) for fatigue strengthening of cracked steel bridge connections. Constr Build Mater 227:116800
7. Maki T, Kobayashi K, Minato M, Tamura I (1984) Thermoelastic martensite in an ausaged Fe–Ni–Ti–Co alloy. Scripta Metall 18(10):1105–1109
8. Sehitoglu H, Zhang X, Kotil T, Canadinc D, Chumlyakov Y, Maier H (2002) Shape memory behavior of FeNiCoTi single and polycrystals. Metall Mater Trans A 33(12):3661–3672
9. Sehitoglu H, Karaman I, Zhang XY, Chumlyakov Y, Maier HJ (2001) Deformation of FeNiCoTi shape memory single crystals. Scripta Mater 44(5):779–784
10. Sohmura T, Oshima R, Fujita FE (1980) Thermoelastic FCC-FCT martensitic transformation in Fe–Pd alloy. Scripta Metall 14(8):855–856
11. Sato A, Chishima E, Soma K, Mori T (1982) Shape memory effect in $\gamma \rightleftarrows \varepsilon$ transformation in Fe-30Mn-1Si alloy single crystals. Acta Metall 30(6):1177–1183
12. Otsuka H, Yamada H, Maruyama T, Tanahashi H, Matsuda S, Murakami M (1990) Effects of alloying additions on Fe–Mn–Si shape memory alloys. ISIJ Int 30(8):674–679
13. Abuzaid W, Sehitoglu H (2018) Superelasticity and functional fatigue of single crystalline FeNiCoAlTi iron-based shape memory alloy. Mater Des 160:642–651
14. Ma J, Hornbuckle B, Karaman I, Thompson G, Luo Z, Chumlyakov YI (2013) The effect of nanoprecipitates on the superelastic properties of FeNiCoAlTa shape memory alloy single crystals. Acta Mater 61(9):3445–3455
15. Karaca H, Turabi A, Chumlyakov Y, Kireeva I, Tobe H, Basaran B (2016) Superelasticity of [001]-oriented Fe426Ni279-Co172Al99Nb2. 4. ferrous shape memory alloys. Scripta Mater 120:54–57
16. Abuzaid W, Sehitoglu H (2019) Shape memory effect in FeMnNiAl iron-based shape memory alloy. Scripta Mater 169:57–60
17. Omori T, Kainuma R (2017) Martensitic transformation and superelasticity in Fe–Mn–Al-based shape memory alloys. Shape Memory Superelast 3(4):322–334
18. Tseng L-W, Ma J, Wang S, Karaman I, Chumlyakov YI (2016) Effects of crystallographic orientation on the superelastic response of FeMnAlNi single crystals. Scripta Mater 116:147–151
19. Omori T, Ando K, Okano M, Xu X, Tanaka Y, Ohnuma I, Kainuma R, Ishida K (2011) Superelastic effect in polycrystalline ferrous alloys. Science 333(6038):68–71
20. Ojha A, Sehitoglu H (2016) Transformation stress modeling in new FeMnAlNi shape memory alloy. Int J Plast 86:93–111
21. Abuzaid W, Wu Y, Sidharth R, Brenne F, Alkan S, Vollmer M, Krooß P, Niendorf T, Sehitoglu H (2019) FeMnNiAl iron-based shape memory alloy: promises and challenges. Shape Memory Superelast 5:263–277
22. Vollmer M, Kriegel M, Walnsch A, Klemm V, Leineweber A, Niendorf T (2019) On the microstructural and functional stability of Fe–Mn–Al–Ni at ambient and elevated temperatures. Scripta Mater 162:442–446
23. Tseng L-W, Ma J, Wang S, Karaman I, Kaya M, Luo Z, Chumlyakov Y (2015) Superelastic response of a single crystalline FeMnAlNi shape memory alloy under tension and compression. Acta Mater 89:374–383

24. Tseng L-W, Ma J, Hornbuckle B, Karaman I, Thompson G, Luo Z, Chumlyakov Y (2015) The effect of precipitates on the superelastic response of [1 0 0] oriented FeMnAlNi single crystals under compression. Acta Mater 97:234–244

25. Tseng L-W, Ma J, Vollmer M, Krooß P, Niendorf T, Karaman I (2016) Effect of grain size on the superelastic response of a FeMnAlNi polycrystalline shape memory alloy. Scripta Mater 125:68–72

26. Omori T, Iwaizako H, Kainuma R (2016) Abnormal grain growth induced by cyclic heat treatment in Fe–Mn–Al–Ni superelastic alloy. Mater Des 101:263–269

27. Omori T, Okano M, Kainuma R (2013) Effect of grain size on superelasticity in Fe–Mn–Al–Ni shape memory alloy wire. APL Mater 1(3):032103

28. Vollmer M, Segel C, Krooß P, Günther J, Tseng L-W, Karaman I, Weidner A, Biermann H, Niendorf T (2015) On the effect of gamma phase formation on the pseudoelastic performance of polycrystalline Fe–Mn–Al–Ni shape memory alloys. Scripta Mater 108:23–26

29. Vollmer M, Krooß P, Karaman I, Niendorf T (2017) On the effect of titanium on quenching sensitivity and pseudoelastic response in Fe–Mn–Al–Ni-base shape memory alloy. Scripta Mater 126:20–23

30. Vollmer M, Arold T, Kriegel M, Klemm V, Degener S, Freudenberger J, Niendorf T (2019) Promoting abnormal grain growth in Fe-based shape memory alloys through compositional adjustments. Nat Commun 10(1):1–10

31. Kajiwara S, Kikuchi T (1983) Reversible movement of the austenite-martensite interface and dislocation structures in reverse-transformed austenite in Fe–Ni–C alloys. Philos Mag A 48(4):509–526

32. Kajiwara S, Owen WS (1977) The martensite-austenite interface and the thickness of twins in martensite in Fe3Pt. Scripta Metallurgica 11(2):137–142

33. Kajiwara S, Kikuchi T (1982) Dislocation structures produced by reverse martensitic transformation in a Cu–Zn alloy. Acta Metall 30(2):589–598

34. Kajiwara S (1999) Characteristic features of shape memory effect and related transformation behavior in Fe-based alloys. Mater Sci Eng A 273:67–88

35. Hirth J, Wang J, Tomé C (2016) Disconnections and other defects associated with twin interfaces. Prog Mater Sci 83:417–471

36. Mohammed ASK, Sehitoglu H (2020) Martensitic twin boundary migration as a source of irreversible slip in shape memory alloys. Acta Mater 186:50–67

37. Vollmer M, Kriegel M, Krooß P, Martin S, Klemm V, Weidner A, Chumlyakov Y, Biermann H, Rafaja D, Niendorf T (2017)

Cyclic degradation behavior of <001>-oriented Fe–Mn–Al–Ni single crystals in tension. Shape Memory Superelast 3(4):335–346

38. Sidharth R, Wu Y, Brenne F, Abuzaid W, Sehitoglu H (2020) Relationship between functional fatigue and structural fatigue of iron-based shape memory alloy FeMnNiAl. Shape Memory Superelast. https://doi.org/10.1007/s40830-020-00283-1

39. McKelvey A, Ritchie R (2001) Fatigue-crack growth behavior in the superelastic and shape-memory alloy Nitinol. Metall Mater Trans A 32(3):731–743

40. Hornbogen E (2004) Review thermo-mechanical fatigue of shape memory alloys. J Mater Sci 39(2):385–399

41. Melton K, Mercier O (1979) Fatigue of NiTi thermoelastic martensites. Acta Metall 27(1):137–144

42. Wu Y, Ojha A, Patriarca L, Sehitoglu H (2015) Fatigue crack growth fundamentals in shape memory alloys. Shape Memory Superelast 1(1):18–40

43. Efstathiou C, Sehitoglu H (2008) Local transformation strain measurements in precipitated NiTi single crystals. Scripta Mater 59(12):1263–1266

44. Gall K, Sehitoglu H, Chumlyakov YI, Kireeva IV (1998) Pseudoelastic cyclic stress-strain response of over-aged single crystal Ti-50.8 at% Ni. Scripta Mater 40(1):7–12

45. Strnadel B, Ohashi S, Ohtsuka H, Miyazaki S, Ishihara T (1995) Effect of mechanical cycling on the pseudoelasticity characteristics of Ti-Ni and Ti-Ni-Cu alloys. Mater Sci Eng A 203(1–2):187–196

46. Simon T, Kröger A, Somsen C, Dlouhy A, Eggeler G (2010) On the multiplication of dislocations during martensitic transformations in NiTi shape memory alloys. Acta Mater 58(5):1850–1860

47. Alkan S, Sehitoglu H (2019) Prediction of transformation stresses in NiTi shape memory alloy. Acta Mater 175:182–195

48. Vollmer M, Krooß P, Kriegel M, Klemm V, Somsen C, Ozcan H, Karaman I, Weidner A, Rafaja D, Biermann H (2016) Cyclic degradation in bamboo-like Fe–Mn–Al–Ni shape memory alloys—the role of grain orientation. Scripta Mater 114:156–160

49. Hamilton RF, Sehitoglu H, Chumlyakov Y, Maier H (2004) Stress dependence of the hysteresis in single crystal NiTi alloys. Acta Mater 52(11):3383–3402

50. Mohammed ASK, Sehitoglu H (2020) Modeling the interface structure of type II twin boundary in B19′ NiTi from an atomistic and topological standpoint. Acta Mater 183:93–109